Enhancing the Force Transparency of the Energy-Reflection Based Time Domain Passivity Approach

Michael Panzirsch[1*], Harsimran Singh[1,2], Xiao Xu[2,3], Alexander Dietrich[1], Thomas Hulin[1,2], Eckehard Steinbach[2,3], Alin Albu-Schaeffer[1]

***Abstract*—The Time Domain Passivity Approach (TDPA) was developed and applied to tackle a variety of control challenges such as non-collocated force sensing, authority scaling or delayed coupling in robotic applications. Specifically for delay, recently, the energy-reflection based TDPA (TDPA-ER) was proposed to improve position tracking and force-feedback quality. In contrast to the conventional TDPA, the TDPA-ER intrinsically prevents position drift, thus, substantially increasing the coupling rigidity. Here, we extend the TDPA-ER, to further enhance the force transparency perceived by the operator in teleoperation scenarios. The extension is based on two independent control strategies which, among others, reorganize the energy distribution of TDPA-ER and ensure more continuous force profiles through the Deflection-Domain Passivity Approach. Experiments confirm the improvement of force-feedback quality and force continuity with regards to TDPA-ER. Furthermore, it is shown that interactions with dynamic objects and active environments can be handled robustly with the proposed teleoperation control strategies.**

***Index Terms*—Tele-robotics, Tele-operation, Deflection-Domain Control**

I. Introduction

THE major control challenge in coupled actuated systems are network delays which potentially lead to instability in the setup. In coupling of autonomous systems, as for landing of aircrafts on a platform [1], [2] or platoons in road traffic [3], mostly position references are exchanged in the communication channel (position-position architecture [4], [5], [6]). In contrast, in tele-operation, for the sake of force transparency, a position command is sent to the robot while the force acting in the robot environment is fed back to the operator side [7], [8]. For optimal force transparency, the interaction force F^E of the robot and its environment should be displayed as accurately as possible on the input device (F^I) with which the operator commands the robot motion.

*Corresponding author

[1]M. Panzirsch (michael.panzirsch@dlr.de), H. Singh (harsimran.singh@dlr.de), T. Hulin (thomas.hulin@dlr.de), A. Dietrich (alexander.dietrich@dlr.de) and A. Albu-Schaeffer (alin.albu-schaeffer@dlr.de) are with the Institute of Robotics and Mechatronics in the German Aerospace Center (DLR), Wessling, Germany.

[2]H. Singh, T. Hulin, X. Xu and E. Steinbach are with the Centre for Tactile Internet with Human-in-the-Loop (CeTI), Cluster of Excellence at TU Dresden, Dresden, Germany

[3]X. Xu (xiao.xu@tum.de) and E. Steinbach (eckehard.steinbach@tum.de) are with the Technical University of Munich; School of Computation, Information and Technology; Chair of Media Technology; Munich Institute of Robotics and Machine Intelligence, Munich, Germany.

Digital Object Identifier (DOI): see top of this page.

Control approaches ensuring stability in case of communication delay often induce a large constant damping or apply adaptive damping. In case of the former, it may be difficult to distinguish between damping and feedback forces, while the latter may lead to disturbances such as sudden drops in the feedback force. Still, when considering coupled systems in tele-operation setups, the force-feedback quality is of utmost importance. The majority of control methods for delayed coupling reduce the force transparency through a velocity-dependent damping force and some potentially result in discontinuous force signals. The latter is a typical artifact of the Time Domain Passivity Approach (TDPA) [9]. The TDPA was applied to enhance the force transparency in explicit force control [10], [8].

While the conventional TDPA [11] ensures passivity and thus stability through attenuation of force-feedback and commanded velocity, the recently presented energy-reflection based TDPA (TDPA-ER, [12], [13], [14]) affects only forces, i. e., the forces commanded to the robot and the force-feedback to the operator. Thus, the TDPA-ER prevents position drift as one of the main transparency-reducing factors in TDPA. Therefore, it was recently elected as part of the IEEE standardization activity P1918.1.1 (aka Haptic Codecs for the Tactile Internet, [15]).

Despite its maturity, some drawbacks of the TDPA remained unsolved so far. Due to the dependency of the control action on the energy flow direction in TDPA, the force-feedback F^I remains unaffected when energy flows from input device to robot (exemplary during the pressing phase of a wall contact), but may suddenly be attenuated by the passivity controllers of the TDPA when the flow direction changes (release phase of a wall contact). We refer to this sudden force drop as *Artifact A1*. This problem arises in all variations of the conventional TDPA [9], its more recent extensions for high delays (TDPA-HD, [16]) and also in TDPA-ER [12]. Another *Artifact A2* of the coupling arises from the fact that the ideal energy level of the energy storage (calculated from spring stiffness and deflection) is different from the observed (passivity-wise available) energy due to delay effects. If the operator moves too fast with respect to the delay, the energy input and, thus, the observed energy is too low such that the passivity controller has to attenuate the robot control force. Since the TDPA-ER acts in the time-domain, the passivity controllers may attenuate the robot control force suddenly completely (*Artifact A2*) as soon as the storage of available energy is emptied. This artifact is

reduced through deflection-domain control in this work.

The major contributions can be summarized to: The presented method substantially enhances the force transparency in TDPA-ER by reducing the force attenuation on the input device side through prescient energy reflection (*Control Strategy I*). Furthermore, the proposed method renders the force attenuation on the robot side more continuous through application of deflection-domain control (*Control Strategy II*).

The paper is structured as follows: Sections II and III introduce the principles of TDPA-ER and the drawbacks of state-of-the-art approaches. The concept and implementation of the proposed method is presented in Section IV. The experimental evaluation for tele-operation with delayed communication and active environments is shown in Section V. The results are discussed in Section VI. Finally, Section VII concludes the work.

II. Fundamentals

The basic Position-Force architecture (PF) of the TDPA-ER was introduced in [12]. Later, it was extended to six degrees-of-freedom (DoF) with the observer-based gradient method (OBG, [17]) and combined with the haptic data reduction approach of [18]. It serves as a passive coupling reference in [19] and was applied in the tele-impedance setup with variable stiffnesses in [20]. A Position-Position architecture (PP) based on TDPA-ER was introduced in [6].

Figure 1 presents the signal flow diagram of the TDPA-ER in a PF architecture. In tele-operation, a human uses an input device to control a robot in a remote environment. Therefore, the position or velocity reference of the input device v^I is transmitted through the communication channel (CC) with forward delay T_f. A deviation between delayed reference $v^{I,del}$ and robot motion v^R is penalized by an impedance controller ($Ctrl$) with spring-damper characteristic. Hereby, the resulting controller force F^C is commanded to the robot and fed back to the input device displaying the delayed force $F^{C,del}$ (with backward delay T_b) to the user.

In TDPA, the energy flow of the system is observed such that excessive energy that potentially leads to instability can be measured and dissipated through adaptive damping. Figure 1 depicts the passivity observer (PO) and the passivity controllers $PC1$ and $PC2$ represented by the variable factors α and β respectively. In contrast to the conventional TDPA [11], the robot-side passivity controller is located on the right of the $Ctrl$ such that both PCs are of impedance causality, i.e. dissipate energy through attenuation of forces (instead of attenuation of $v^{I,del}$ in the conventional TDPA).

The passivity observers PO_L, PO_M, and PO_R indicate where the energy flow is measured in TPDA-ER. These locations correspond to the ports 2, 4 and 5 of Fig. 2 presenting the control concept of TDPA-ER in more detail. Note that the red marked elements represent the proposed enhancement and can be neglected in the beginning. At each port i of this network representation, the power can be calculated in each time step k from force (effort variable) and velocity (flow variable): $P^i(k) = v^i(k)F^i(k)$. From the sign of the power, the direction of power flow in left-to-right direction (L2R) and right-to-left direction (R2L) can be determined:

$$P^i_{L2R}(k) = \begin{cases} 0, & \text{if } P^i(k) \leq 0 \\ P^i(k), & \text{if } P^i(k) > 0, \end{cases} \tag{1}$$

$$P^i_{R2L}(k) = \begin{cases} 0, & \text{if } P^i(k) \geq 0 \\ -P^i(k), & \text{if } P^i(k) < 0. \end{cases} \tag{2}$$

Note that the sign of the flow direction depends on the sign convention in $Ctrl$. With sampling time T_s, the energies can be calculated via integration: $E^i_{L2R}(k) = T_s \sum_{j=0}^{k} P^i_{L2R}(j)$ and $E^i_{R2L}(k) = T_s \sum_{j=0}^{k} P^i_{R2L}(j)$. From the network scheme, it becomes obvious that the TDPA-ER ensures passivity of the whole delayed 2-port including CC and $Ctrl$. Thereby, the impedance controller $Ctrl$ can be considered as an energy storage element that mainly represents the potential energy E_{pot} in the spring load of the controller. While the ideal energy storage of the $Ctrl$ is the sum of input and output energy of the 2-port $Ctrl$ in Fig. 2, the available energy in the monitoring unit is charged from the input energies flowing in left-to-right direction E^1_{L2R} at port 1 and in right-to-left direction E^6_{R2L} at port 6. The monitoring unit distributes the available energy $E_{R2L,des}$ and $E_{L2R,des}$ to port 1 and port 6 as a reference for the respective passivity controllers. The PCs limit the output energy according to these references to ensure passivity of the 2-port. The energy storage E_{st} of the monitoring unit is calculated as:

$$\begin{aligned} E_{st}(k) = {} & E_{st}(k-1) + E^1_{L2R}(k - T_f) \\ & - E^1_{L2R}(k - T_f - 1) + E^6_{R2L}(k) - E^6_{R2L}(k-1) \\ & - P_{R2L,des}(k)T_s - P_{L2R,des}(k)T_s. \end{aligned} \tag{3}$$

In TDPA-ER, so far, the energy was distributed in a proportional way in accordance to the current output power on each side of the $Ctrl$ 2-port. Therefore, the current output power P^{act}_{out} of the $Ctrl$ was calculated as: $P^{act}_{out}(k) = P^4_{R2L}(k) + P^5_{L2R}(k)$, with

$$P_{exc}(k) = E_{st}(k)/T_s - P^{act}_{out}(k), \tag{4}$$

which is the excessive power which leaves $Ctrl$ but is not available in the energy storage E_{st}. The desired power output in L2R and R2L direction was then distributed in a proportional manner:

$$P_{R2L,des}(k) = \begin{cases} P^4_{R2L}(k) & +P_{exc}(k)\frac{P^4_{R2L}(k)}{P^{act}_{out}(k)}, \\ & \text{if } \frac{E_{st}(k)}{T_s} \leq P^{act}_{out}(k) \\ P^4_{R2L}(k), & \text{if } \frac{E_{st}(k)}{T_s} > P^{act}_{out}(k), \end{cases} \tag{5}$$

$$P_{L2R,des}(k) = \begin{cases} P^5_{L2R}(k) & +P_{exc}(k)\frac{P^5_{L2R}(k)}{P^{act}_{out}(k)}, \\ & \text{if } \frac{E_{st}(k)}{T_s} \leq P^{act}_{out}(k) \\ P^5_{L2R}(k), & \text{if } \frac{E_{st}(k)}{T_s} > P^{act}_{out}(k). \end{cases} \tag{6}$$

From these powers, $E_{R2L,des}$ and $E_{L2R,des}$ are determined via integration.

The OBG 2-port in Fig. 2 introduces the observer-based gradient method [17]. The OBG was proposed to enhance the force transparency by reducing the high frequency oscillations of the impedance type $PC2$ and especially to preserve the physical behavior of the coupling controller with spring characteristics despite delay [21]. Therefore, it rectifies the

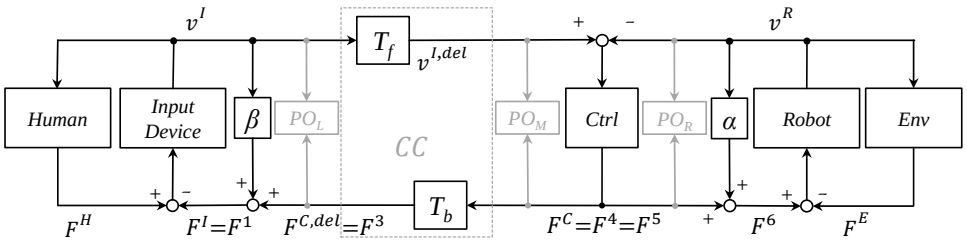

Fig. 1: Signal flow diagram of a TDPA-ER position-force computed architecture.

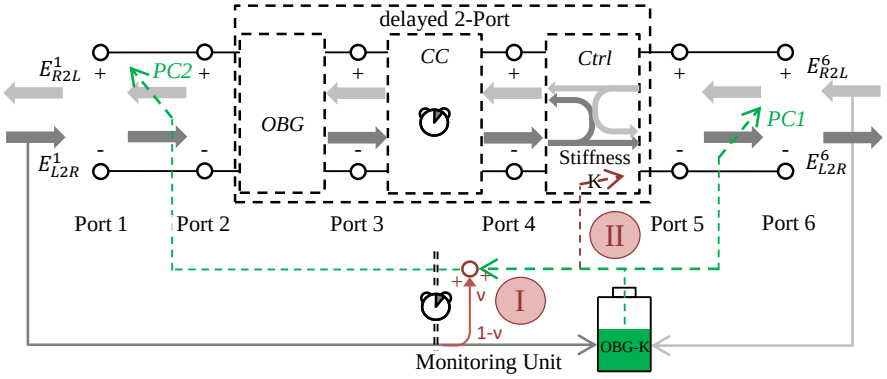

Fig. 2: Proposed enhanced concept of TDPA-ER.

feedback force F^3 on the operator side such that the force-feedback behaves analogous to the motion command. Thereby, the OBG method acts on the deflection-domain independent of time, in contrast to the TDPA based on the time-domain. The reader is referred to [21] for a detailed description of the OBG method.

III. Problem Statement

The bilateral teleoperation experiment in Fig. 3 depicts a free motion and wall contact with TDPA-ER and OBG at 100ms round-trip delay (RTD). Figure 4 and Fig. 5 present the respective experimental setup that is further described in Section V. The position tracking of input device (x^I) and robot (x^R) is of high quality despite the high delay since position drift is prevented by TDPA-ER. *Still, for the sake of passivity, due to delayed power flow in R2L direction, $PC2$ attenuates F^2 to F^1 already at $t \in [9.5s, 10.7s]$ (**Artifact A1** of the TDPA).* When the input device starts commanding the release of the wall contact at about $t_1 = 9.5s$, the allowed output power flow at port 1 is $P^1_{R2L,des}(k) = P^4_{R2L,des}(k - T_b) = 0$. At $t_1 + T_f = 9.55s$, the power flow at port 4 changes the sign such that $P^4_{R2L,des} \neq 0$, while $P^1_{R2L,des}$ at port 1 turns non-zero at $t_1 + T_f + T_b = 9.6s$. I.e., during $t \in [t_1, t_1 + T_f + T_b]$, $PC2$ dissipates the power leaving in R2L direction which results in a strong force attenuation as visible in the respective plot. Due to this force reduction, an operator that wants to slowly reduce the wall contact (i.e. via slow reduction of the pressing force) might drop back into the wall penetration as can be seen in the position (maximum deflection at $10s$ after $t = t_1 + T_f + T_b$). The resulting deflection of the coupling spring can also be analyzed from the passivity confirming energy plot E_{PP} (the sum of in- and output energies at port 1 and 6) at $t \in [9.5s, 10.7s]$. In contrast, $PC1$ only slightly attenuates the force F^4 commanded to the robot. *The sudden*

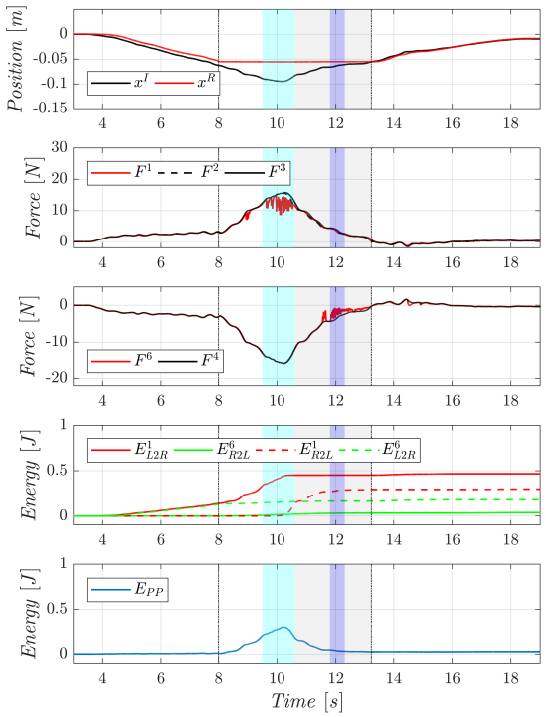

Fig. 3: Performance of TDPA-ER with OBG at 100ms RTD: experiment with free motion and wall contact. F^1: displayed to the input device, F^2: OBG output to $PC2$, F^3: received at the operator side, F^4: output of the coupling controller, F^6: commanded to the robot. Light-shaded area marks main $PC2$, dark-shaded area main $PC1$ attenuation. F^δ_I: 8.9%, F^δ_R: 3.8%.

Fig. 4: Force Dimension's lambda.7

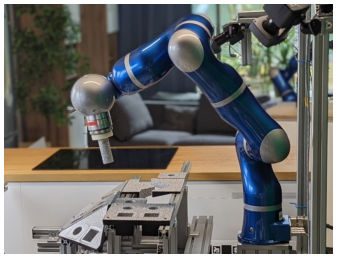

Fig. 5: DLR's light-weight robot

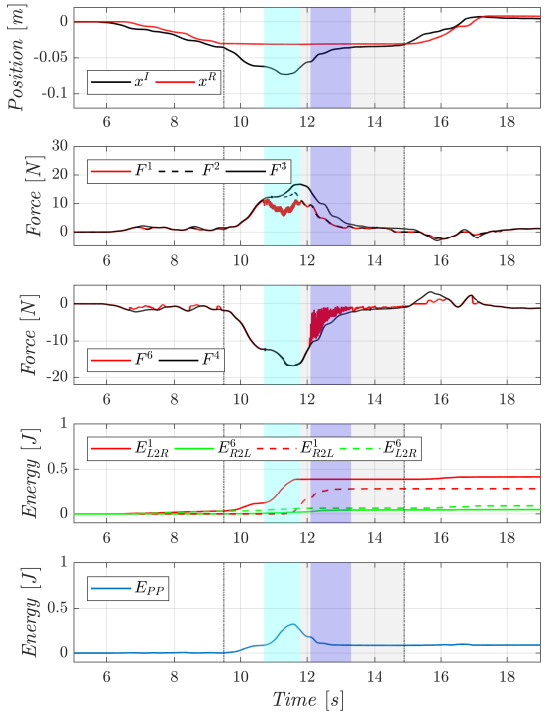

Fig. 6: Performance of TDPA-ER with OBG at 400ms RTD. F_I^δ: 50.4%, F_R^δ: 11%.

strong dissipation by $PC1$ results from ***Artifact A2****, i.e. the time-domain method does not forecast when no energy will be left in the storage during one spring deflection phase.* Therefore, when the storage E_{st} is empty, but not earlier, the output is adapted. This *Artifact A2* cannot be solved in the time-domain, but – as will be shown later – in the deflection-domain.

The metrics F_I^δ and F_R^δ present the percental force attenuation during the wall contact phase and are defined as $F_I^\delta = \frac{F^3-F^1}{F_3}$ and $F_R^\delta = \frac{F^4-F^6}{F_4}$. The control strategies proposed in the course of this work aim for lowering the value of these metrices. In the experiment based on the conventional TDPA-ER in Fig. 3, F_I^δ=50.4% and F_R^δ=11%.

In the corresponding experiment with 400ms RTD (see Fig. 6), the force attenuation of $PC2$ at $t \in [10.7s, 11.8s]$ starts with a release motion of the operator at $t = 10.7s$. But, this attenuation again leads to a drop of the operator into the spring (maximum deflection at $t = 11.4s$). From the energy E_{PP} serving the passivity confirmation, this drop can be analyzed from an injection of additional energy.

IV. Proposed Approach

As described above, the TDPA-ER considers the robot-side impedance controller in the passivity-controlled subsystem as an energy storage. This energy storage is the technological aspect of TDPA-ER that enables the proposed force transparency enhancement: The TDPA-ER stores the available energy (which the system may eject without violating passivity) in a monitoring unit on the robot side. The available energy is then distributed to the robot or input device side according to the current power flow. Here, we propose to reflect a part E^ν of the available energy directly to the input device side in advance to prevent sudden force drops when the energy flow direction changes (*Artifact A1*). Thereby, no assumptions or predictions on the energy behavior are required, since the passivity controller setup of TDPA-ER intrinsically ensures passivity of the delayed coupling 2-port. *Artifact A2*, described above, results from the difference between ideal energy level and observable energy. To reduce this artifact, the Deflection-Domain Passivity Approach (DDPA, [20]) is adopted here. The DDPA was developed to ensure passivity of variable stiffnesses (as an alternative to time-domain control [22]) through adaptation of the coupling stiffness over the deflection of the coupling spring. Here, the DDPA is introduced to adapt the stiffness and thus the control force over the spring deflection in a predictive manner and therefore earlier and more continuously than through time-domain control.

A. Reducing Artifact A1 through Control Strategy I

1) Concept Description: Figure 2 depicts the proposed energy distribution concept – *Control Strategy I* (encircled I) – reducing *Artifact A1*. As discussed above, *Artifact A1* mainly appears during wall contacts and due to delayed information of energy reflection. In theory, in case of a rigid wall contact, the full potential energy stored in the spring is reflected back to the operator due to zero velocity of the robot. Knowing this, during a wall contact, the energy arriving from the input device E_{L2R}^3 could be completely reflected back even before the wall contact is released. Then, the $PC2$ dissipation is substantially reduced (in case of velocities appropriate for the respective RTD) and *Artifact A1* can be eliminated completely.

But, to increase robustness in case of non-steady environments (e.g. a suddenly vanishing rigid wall as simulated in the experiments below), with *Control Strategy I*, we propose to reflect only a proportion ν of the energy E^ν in advance as depicted in Fig. 2 (encircled I). Furthermore, ν can be arbitrarily varied online. For example, ν can be reduced as long as the spring deflection of the coupling controller is below a certain threshold δ^{th} (implying a free/unhindered robot motion). Still, note that for all values of $\nu = [0, 1]$ passivity of the 2-port will be ensured by the passivity controllers.

2) Implementation: The proposed prescient reflection of energy is implemented as follows: The new energy storage E_{st}^* has to be calculated as:

$$\begin{aligned} E_{st}^*(k) = E_{st}^*(k-1) + (1-\nu)(E_{L2R}^1(k-T_f) - \\ E_{L2R}^1(k-T_f-1)) + E_{R2L}^6(k) - E_{R2L}^6(k-1) - \\ P_{R2L,des}(k-1)T_s - P_{L2R,des}(k-1)T_s. \end{aligned} \quad (7)$$

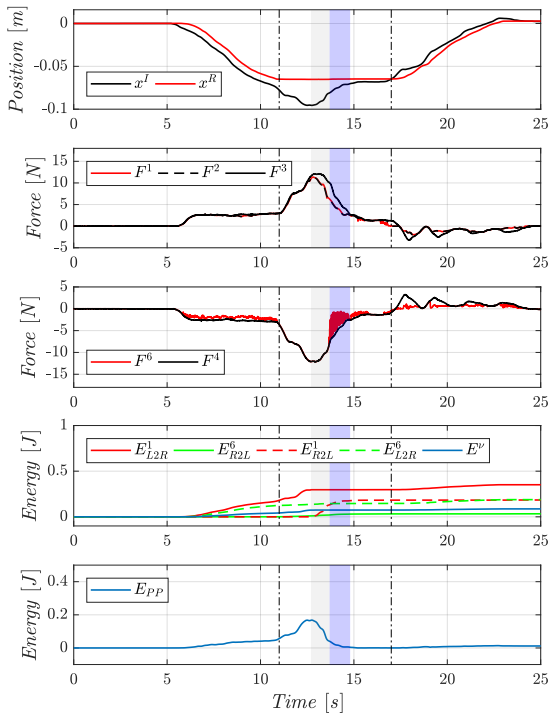

Fig. 7: Performance of TDPA-ER with OBG and Strategy I (E_ν) at 400ms RTD. F_I^δ: 17.4%, F_R^δ: 9.2%.

In addition, the allowed output energy $E^*_{R2L,des}$ on the input device side changes to:

$$E^*_{R2L,des}(k) = E_{R2L,des}(k) + \nu E^1_{L2R}(k - T_f), \qquad (8)$$

where $E_{R2L,des}(k)$ is the time integrative of $P_{R2L,des}(k)$ which results from the new stored energy E^*_{st} of (7) analogous to (5). Thereby, P_{exc} is found from E^*_{st} analogous to (4).

Despite adaptation of ν (e.g. $\nu = 0$ at $\delta(k) < \delta^{th}$), in special situations, the performance on the robot side is potentially reduced through *Control Strategy I*. For instance, when an object in the environment is non-static, in case of stiction, energy that has already been reflected to the operator side through ν might be missing on the robot side for the respective robot motion. In such situations, *Artifact A2* may be engraved. Therefore, ν-variation should also depend on the velocity v^R of the robot, such that $\nu = 0$, if $\delta(k) < \delta^{th}$ OR $v^R(k) > v^{th}$, with a velocity threshold v^{th} indicating a contact with a steady environment. Note that for the following experiments, ν was set to 0.25 and the deflection and velocity threshold were chosen as $\delta^{th} = 1mm$ and $v^{th} = 5mm/s$. In the experimental setup of this work, this was evaluated as a subjectively rated optimal configuration to reduce the $PC2$ dissipation during wall contacts and $PC1$ dissipation during free motion phases.

Figure 7 presents an experiment with OBG and *Control Strategy I* at 400ms RTD. The benefit of *Control Strategy I* becomes visible at maximum spring deflection at $t = 12.7s$. Here, $PC2$ does not attenuate the force-feedback such that the operator does not drop into the spring. This also becomes obvious from the non-raising energy E_{PP}. Although, $PC1$ is expected to dissipate more energy due to *Control Strategy I* and the resulting reflection of energy E_ν, the dissipation is not substantially stronger than in the corresponding experiment without *Control Strategy I* of Fig. 6 (compare dark shaded area at $t \in [13.7s, 14.8s]$ and metric F_R^δ).

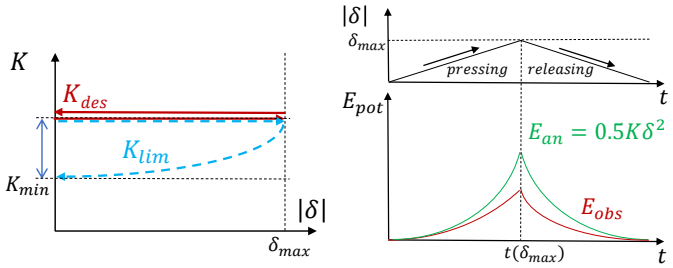

(a) Stiffness attenuation to K_{lim} during releasing phase.

(b) Spring deflection, analytical E_{an}, and observed energy E_{obs}.

Fig. 8: The Deflection-Domain Passivity Approach: Due to delay, the observed energy E_{obs} is charged up less than the analytical energy E_{an} during the pressing phase. To ensure passivity, the DDPA designs a stiffness curve K_{lim} for the release phase that ensures passivity with $E_{obs} \geq 0$.

B. Reducing Artifact A2 through Control Strategy II

1) Concept Description: In [20], the deflection-domain passivity approach was introduced to ensure passivity of variable stiffnesses for arbitrary stiffness profiles. Since for variable stiffnesses, the observed energy of the spring may be much lower than the analytical potential energy $E_{an}(k) = 0.5K(x^I(k) - x^R(k))^2$, passivity potentially requires the full attenuation of the commanded forces from an unpredictable point in time during one spring deflection phase in case of time-domain control (compare *Artifact A2*).

The main control principle of DDPA is the control of the energy output of the coupling controller $Ctrl$ over its deflection. This can be realized by reducing the $Ctrl$ stiffness K_{des} to K_{lim} to influence the energy output of a spring from the beginning of the spring release phase. Thereby, the energy reference is observed at port 4 and 5 of $Ctrl$ (see Fig. 2) over time.

Here, DDPA is applied to reduce *Artifact A2* by reducing the stiffness maximally to a threshold K^{min} during the release phase of a spring deflection in a predictive manner. The concept is marked as an encircled II in Fig. 2. The working principle of DDPA is described in Fig. 8 in more detail. In this work, we assume a constant impedance controller stiffness $K_{des} = K_c$. Via DDPA, a polynomial stiffness function K_{lim} is designed according to the available energy E_{obs} which limits the controller stiffness from the beginning of the spring release phase (maximum spring deflection) if $E_{obs} < E_{an} = 0.5K_c(x^I(k - T_f) - x^R(k))^2$. This leads to a continuous energy dissipation during the spring release phase.

2) Implementation: Here, due to the reflection of energy E^ν, the reference energy E_{obs} of the DDPA equals E^*_{st} from (7). From here, $\delta(k) = |x^{I,del}(k) - x^R(k)|$ describes the absolute value of the spring deflection, with the delayed input device pose $x^{I,del}$ (integral of $v^{I,del}$) on the robot side. δ_{max} describes the time-varying maximal deflection and K_{lim}

the applied attenuated stiffness. Analogous to the equations of [20], a nonlinear limiting function K_{lim}^{pol} is calculated in each time step during a deflection phase which ensures that $E_{obs}(k) \geq 0$:

$$K_{lim}^{pol}(\delta) = \frac{K_{k1} - K_{zero} - \frac{3E_{obs}(\delta_{k1})}{\delta_{k1}^2} + \frac{3K_{zero}}{2}}{\delta_{k1}^d(1-\frac{3}{d+2})}\delta^d + \frac{E_{obs}(\delta_{k1}) - \frac{a}{d+2}\delta_{k1}^{d+2} - \frac{K_{zero}}{2}\delta_{k1}^2}{\frac{1}{3}\delta_{k1}^3}\delta + K_{zero}, \tag{9}$$

$$\text{with} \quad a = \frac{K_{k1} - c - \frac{3E_{obs}(\delta_{k1})}{\delta_{k1}^2} + \frac{3c}{2}}{\delta_{k1}^d(1-\frac{3}{d+2})}, \tag{10}$$

$$b = \frac{E_{obs}(\delta_{k1}) - \frac{a}{d+2}\delta_{k1}^{d+2} - \frac{c}{2}\delta_{k1}^2}{\frac{1}{3}\delta_{k1}^3}, \tag{11}$$

and $c = K_{zero}$. Here, $k1$ is the instant of calculation of K_{lim}^{pol} and thus, the instant in which $K_{k1} = K_c$, $E_{obs}(\delta_{k1}) = E_{obs}(k1)$ and $\delta_{k1} = \delta(k1)$ are measured. Here, the exponent d of the polynomial limiting function was set to $d = 2$ throughout the experiments and K_{zero} equals K_c. The applied stiffness K_{act} is limited as follows: $K_{act} = min(max(K_{lim}, K_{min}), K_c)$. If this stiffness K_{min} is insufficient to ensure passivity, $PC1$ will dissipate energy through attenuation of the force at port 4. The reader is referred to [20] for more details on the implementation of the DDPA. Note that while the force resulting from K_{act} is applied to the robot, here, the force-feedback is still computed from K.

C. Passivity Discussion

Passivity is guaranteed if less energy exits than was introduced into the 2-port: $E_{L2R}^1(k) + E_{R2L}^6(k) \geq E_{R2L}^1(k) + E_{L2R}^6(k)$. The passivity discussion of the enhanced TDPA-ER can be split in three parts. Still, it has to be mentioned that the passivity controllers of the conventional TDPA-ER are sufficient to ensure passivity.

- TDPA-ER: The energy distribution in the energy monitoring unit Equ. (3)-(7) ensures that not more energy than has entered the 2-port is distributed to the left and right side output E_{L2R}^{des} and E_{R2L}^{des}: $E_{R2L}^{des}(k) + E_{L2R}^{des}(k) \leq E_{L2R}^1(k) + E_{R2L}^6(k)$.
  The passivity controllers PC2 and PC1 ensure that not more energy than $E_{R2L}^{des}(k)$ and $E_{L2R}^{des}(k)$ leave at port 1 and port 6: $E_{R2L}^1 \leq E_{R2L}^{des}(k - T_b)$ and $E_{L2R}^6 \leq E_{L2R}^{des}(k)$.
  These equations ensure passivity since the respective energies are monotonously increasing.
- *Control strategy I*: The ν-reflection approach varies the energy distribution of the energy monitoring unit while the overall distributed energy is not varied. The energy $\nu E_{L2R}^1(k)$ is reflected directly back to the left side. Therefore, the energy that may be distributed to both sides by the energy monitoring unit with energy storage (3) is reduced by $\nu E_{L2R}^1(k)$ in (7).
- *Control strategy II*: The variation of $Ctrl$ stiffness K through the DDPA has no influence on passivity since it serves as a preceding dissipation of energy before $PC1$. In case the DDPA does not dissipate sufficient energy, more energy is dissipated by $PC1$ alternatively.

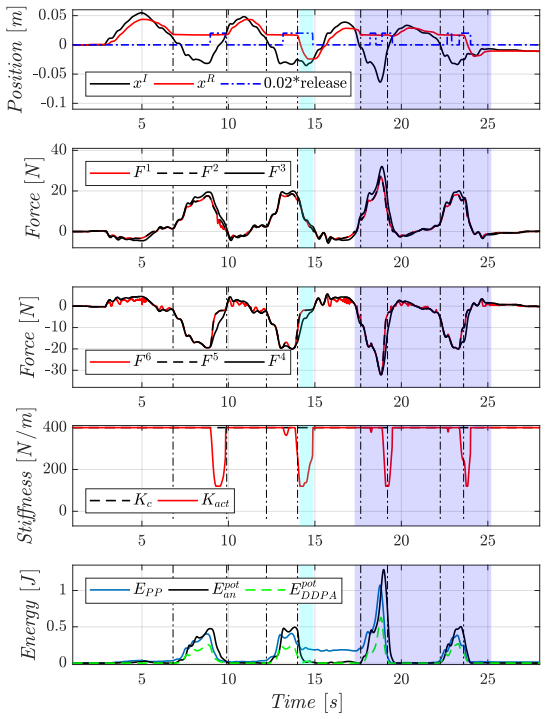

Fig. 9: TDPA-ER with OBG and Control Strategies I and II at 100ms RTD: Only the force F^5 sent to the robot is altered through DDPA. F_I^δ: 19.3%, 7.8%, 25.1%, 10.2%, F_R^δ: 12.9%, 3.4%, 10.4%, 5.6%.

V. Experimental Evaluation

All experiments were performed with the input device lambda.7 of Force Dimension (compare Fig. 4) and a DLR light-weight robot (LWR, see Fig. 5). The control software was implemented with Matlab/Simulink and executed on a rtLinux system at 1kHz sampling rate. The presented control approach was implemented only in z-direction such that only 1-degree of freedom (DoF) plots are presented.

The experiments in Fig. 9 and Fig. 10 present the combination of TDPA-ER, OBG and the proposed *Control Strategies I* and *II* for 100ms and 400ms RTD. The last experiment (see Fig. 11) evaluates the robustness against active environments among others. For the experiments, the deadzone of the DDPA, in which energies and stiffness are reset, was set to $1mm$. Since the DDPA performs better with increasing stiffness, the stiffness was set to $K_c = 400N/m$ (as for the preceding experiments).

The experiment with 100ms RTD (compare Fig. 9) presents free motion and wall contacts with slow velocities at $t \in [2s, 17s]$ and fast velocities at $t \in [17s, 26s]$ (dark shaded area). During the second wall contact, the robot is moved

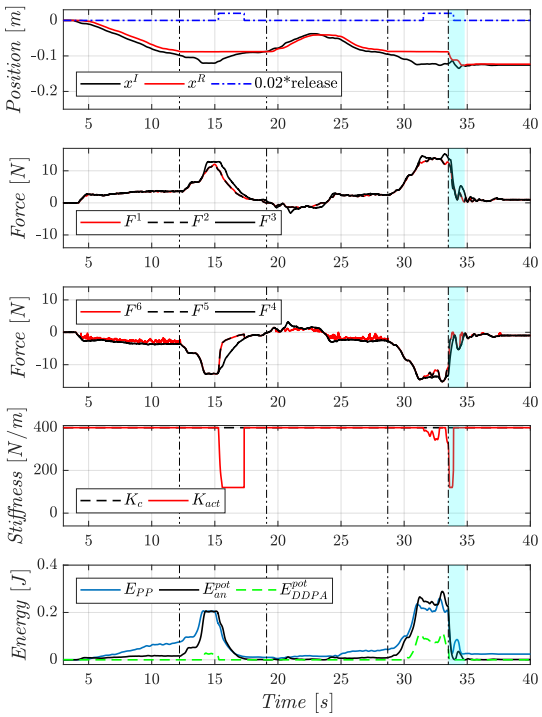

Fig. 10: TDPA-ER with OBG and Control Strategies I and II at 400ms RTD. F_I^δ: 19.5%, 5.7%, F_R^δ: 23.8%, 3.9%.

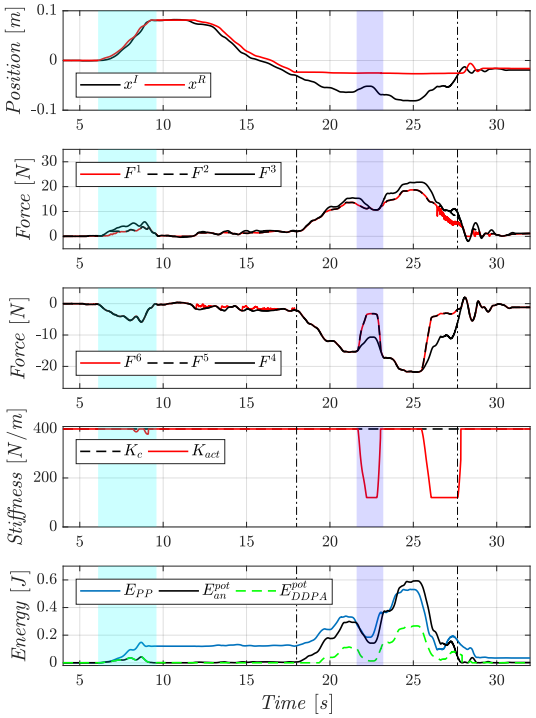

Fig. 11: Performance of TDPA-ER with OBG, Strategies I and II at 400ms RTD with active environment (light-shaded area) and complex interactions during contact (dark-shaded area). F_I^δ: 17.3%, F_R^δ: 22.3%.

in x-direction such that the robot drops into a hole in z-direction (compare light shaded area $t \in [14.1s, 14.9s]$). This procedure serves a robustness test of the proposed approach since the robot might get stuck in motion when not enough energy is available on the robot side due to *Control Strategy I*. The drop is repeated during the last wall contact. It can be observed that throughout the motion at varying velocities, the position tracking is of adequate quality regarding the delay. Both passivity controllers dissipate only very little energy. During all wall contacts, the dissipation by DDPA is sufficient such that $PC1$ does not need to further alter F^5.

During the experiments with 400ms RTD (see Fig. 10), the velocity command was reduced to velocities adequate to the delay range. The dissipation of the passivity controllers is not increased when compared to the preceding experiment at 100ms RTD. The effect of the DDPA is well visible in the plots of F^5 and K_{act}. Without DDPA, $PC1$ would have led to a long phase of full force attenuation during wall contacts. As before, during $t \in [33.5s, 34.8s]$, the robot drops into a hole due to a motion in x-direction (light shaded area). Since the position convergence is satisfactory throughout the experiment, the robustness of the proposed control strategies is confirmed.

The final experiment presented in Fig. 11 serves as a robustness test at 400ms RTD. The light shaded area (see $t \in [6.1s, 9.6s]$) presents a phase with an active environment where the robot is moved by a human and the input device follows. Note that the asymmetric PF architecture is not optimal for this reversed setup. Since, in this phase, the coupling controller is located on the leading agent's side, step-wise motions result. The DDPA adapts the stiffness only slightly. During the wall contact of the robot, the operator repetitively reduces and increases the deflection at $t \in [21.6, 23.2s]$ (dark shaded area). During this variation of deflection, the DDPA correctly varies the stiffness according to the polynomial function. Thus, also robustness in complex interactions is confirmed.

VI. Discussion

The experiments showed that the phases of intense force attenuation were efficiently reduced through the proposed control methods. This is especially obvious for the operator side (compare metrics F_I^δ). The metric F_R^δ shows that the attenuation on the robot side depends on the delay as well as on the behavior of the operator. Future work should investigate the optimal choice of ν in this regard.

Here, we proposed discrete changes of ν depending on the spring deflection and the robot velocity. Too high ν values may lead to energy gaps on the robot side, while too low values may not sufficiently reduce *Artifact A1*. In case of hard contacts, ν can be chosen high while lower values are recommended if movable objects are applied. In such environments, adaptive ν designs adapting to the robot velocity, for instance, can prove favourable. Furthermore, the effect of ν-reflection is reduced if the devices are moved too fast with respect to the delay size. These variables need to be considered when analyzing optimal ν designs in future work.

Although also filters might reduce the force jitter at the cost of slightly active behavior (low-pass filters) or additional

masses and dampers [23], they can neither prevent the force drop on the operator side nor act in a predictive manner as the DDPA. It has to be noted that also the proposed methods can only lead to high performance in case of motion demands at velocities adequate to the delay value.

Here, the robustness in case of complex environments was shown in case of suddenly disappearing contacts. In this extreme case, the convergence to the reference pose was ensured through adaptive design of the ν-reflection (compare Fig. 9 and Fig. 10). Analogously, the control strategies I and II promise a high coupling performance in case of interactions with real world objects. Furthermore, the robustness in case of active environments was evaluated in the experiment of Fig. 11. The experimental validation has shown that the adaptation of ν depending on the robot velocity (to differ more precisely between free motion and wall contacts) improves the system performance.

The results promise that the proposed methods can robustly handle more complex dynamic environments e.g. when lifting weights or when pushing objects such as doors with nonlinear resistance characteristics.

VII. Conclusion and Future Work

In this work, two control strategies were proposed to enhance the force transparency of the TDPA-ER through prescient energy reflection and deflection-domain passivity control. *Control Strategy I* reduced the attenuation of the force-feedback through the TDPA-ER passivity controller substantially, while *Control Strategy II* rendered the force command to the robot more continuous. The experiments confirmed the robustness against active environments and repetitive pressing phases during wall contacts among others. In future work, the applicability of the proposed methods to the position-position architecture of TDPA-ER [6], the compatibility with the haptic data reduction approach of [18] and the effects of actuator limitations [24] should be investigated. Furthermore, the optimal parametrization of the proposed *Control Strategies I* and *II* should be identified for a variety of scenarios and delay values.

Acknowledgment

The research work was partially funded by the German Research Foundation (DFG, Deutsche Forschungsgemeinschaft) as part of Germany's Excellence Strategy – EXC 2050/1 – Project ID 390696704 – Cluster of Excellence "Centre for Tactile Internet with Human-in-the-Loop" (CeTI) of Technische Universität Dresden. The work was partially funded by the Bavarian Ministry of Economic Affairs, Regional Development and Energy, within the project SMiLE2gether(LABAY102).

References

[1] T. Muskardin, A. Coelho, E. R. Della Noce, A. Ollero, and K. Kondak, "Energy-Based Cooperative Control for Landing Fixed-Wing UAVs on Mobile Platforms Under Communication Delays," *IEEE RAL*, vol. 5, no. 4, pp. 5081–5088, 2020.

[2] M. Maier, A. Oeschger, and K. Kondak, "Robot-assisted landing of VTOL UAVs: Design and comparison of coupled and decoupling linear state-space control approaches," *IEEE RAL*, vol. 1, no. 1, pp. 114–121, 2015.

[3] C. Bergenhem, S. Shladover, E. Coelingh, C. Englund, and S. Tsugawa, "Overview of platooning systems," in *Proceedings of the 19th ITS World Congress, Oct 22-26, Vienna, Austria (2012)*, 2012.

[4] V. Chawda and M. K. O'Malley, "Position synchronization in bilateral teleoperation under time-varying communication delays," *IEEE/ASME Transactions on Mechatronics*, vol. 20, no. 1, pp. 245–253, 2015.

[5] H. Singh, M. Panzirsch, A. Coelho, and C. Ott, "Proxy-based approach for position synchronization of delayed robot coupling without sacrificing performance," *IEEE RAL*, vol. 5, no. 4, pp. 6599–6606, 2020.

[6] M. Panzirsch and H. Singh, "Position synchronization through the energy-reflection based time domain passivity approach in position-position architectures," *IEEE RAL*, vol. 6, no. 4, pp. 7997–8004, 2021.

[7] G. Niemeyer and J.-J. Slotine, "Towards force-reflecting teleoperation over the internet," in *Proceedings. 1998 IEEE ICRA*, vol. 3. IEEE, 1998, pp. 1909–1915.

[8] R. Balachandran, J.-H. Ryu, M. Jorda, C. Ott, and A. Albu-Schaeffer, "Closing the force loop to enhance transparency in time-delayed teleoperation," in *2020 IEEE ICRA*. IEEE, 2020, pp. 10 198–10 204.

[9] J.-H. Ryu and C. Preusche, "Stable bilateral control of teleoperators under time-varying communication delay: time domain passivity approach," in *IEEE International Conference on Robotics and Automation*. IEEE, 2007, pp. 3508–3513.

[10] M. Jorda, R. Balachandran, J.-H. Ryu, and O. Khatib, "New passivity observers for improved robot force control," in *2017 IEEE/RSJ IRO)*. IEEE, 2017, pp. 2177–2184.

[11] J. Artigas, J.-H. Ryu, and C. Preusche, "Position drift compensation in time domain passivity based teleoperation," in *IEEE/RSJ IROS*. IEEE, 2010, pp. 4250–4256.

[12] M. Panzirsch, J.-H. Ryu, and M. Ferre, "Reducing the conservatism of the time domain passivity approach through consideration of energy reflection in delayed coupled network systems," *Mechatronics*, vol. 58, pp. 58–69, 2019.

[13] M. Panzirsch, H. Singh, and C. Ott, "The 6-dof implementation of the energy-reflection based time domain passivity approach with preservation of physical coupling behavior," *IEEE RAL*, vol. 5, no. 4, pp. 6756–6763, 2020.

[14] M. Panzirsch, T. Hulin, J. Artigas, C. Ott, and M. Ferre, "Integrating measured force feedback in passive multilateral teleoperation," in *Haptics: Perception, Devices, Control, and Applications*. Springer, 2016, pp. 316–326.

[15] E. Steinbach, M. Strese, M. Eid, X. Liu, A. Bhardwaj, Q. Liu, M. Al-Ja'afreh, T. Mahmoodi, R. Hassen, A. El Saddik *et al.*, "Haptic codecs for the tactile internet," *Proceedings of the IEEE*, vol. 107, no. 2, pp. 447–470, 2018.

[16] M. Panzirsch, A. Pereira, H. Singh, B. Weber, E. Ferreira, A. Gherghescu, L. Hann, E. den Exter, F. van der Hulst, L. Gerdes *et al.*, "Exploring planet geology through force-feedback telemanipulation from orbit," *Science Robotics*, vol. 7, no. 65, 2022.

[17] H. Singh, A. Jafari, and J.-H. Ryu, "Enhancing the force transparency of time domain passivity approach: Observer-based gradient controller," in *IEEE ICRA*. IEEE, 2019, pp. 1583–1589.

[18] X. Xu, M. Panzirsch, Q. Liu, and E. Steinbach, "Integrating haptic data reduction with energy reflection-based passivity control for time-delayed teleoperation," in *2020 IEEE Haptics Symposium (HAPTICS)*. IEEE, 2020, pp. 109–114.

[19] R. Balachandran, H. Mishra, M. Panzirsch, and C. Ott, "A finite-gain stable multi-agent robot control framework with adaptive authority allocation," in *2021 IEEE ICRA*. IEEE, 2021, pp. 1579–1585.

[20] M. Panzirsch, M. Sierotowicz, R. Prakash, H. Singh, and C. Ott, "Deflection-domain passivity control of variable stiffnesses based on potential energy reference," *IEEE RAL*, vol. 7, no. 2, pp. 4440–4447, 2022.

[21] H. Singh, M. Panzirsch, and J.-H. Ryu, "Preserving the physical coupling in teleoperation despite time delay through observer-based gradient control," *IFAC-PapersOnLine*, vol. 52, no. 18, pp. 25–30, 2019.

[22] M. Laghi, A. Ajoudani, M. G. Catalano, and A. Bicchi, "Unifying bilateral teleoperation and tele-impedance for enhanced user experience," *IJRR*, vol. 39, no. 4, pp. 514–539, 2020.

[23] J.-H. Ryu, J. Artigas, and C. Preusche, "A passive bilateral control scheme for a teleoperator with time-varying communication delay," *Mechatronics*, vol. 20, no. 7, pp. 812–823, 2010.

[24] F. Porcini, A. Filippeschi, M. Solazzi, C. A. Avizzano, and A. Frisoli, "Actuator capabilities aware limitation for tdpa passivity controller action," in *2023 IEEE ICRA*. IEEE, 2023, pp. 12 058–12 064.